Solar Energy 179 (2019) 326–334

Contents lists available at ScienceDirect

Solar Energy

journal homepage: www.elsevier.com/locate/solener

Dynamic electro-thermal modeling of solar cells and modules

Pierluigi Guerriero[a,*], Lorenzo Codecasa[b], Vincenzo d'Alessandro[a], Santolo Daliento[a]

[a] Department of Electrical Engineering and Information Technology, University of Naples Federico II, 80125 Naples, Italy
[b] Department of Electronics, Information, and Bioengineering, Politecnico di Milano, Milan, Italy

ARTICLE INFO

Keywords:
Electro-thermal
Hot spot
Partial shading
PV modeling

ABSTRACT

An accurate model describing the electro-thermal behavior of solar modules, subject to varying irradiance conditions, is presented. The model relies on an enhanced version of the popular one-diode model, implementing the temperature dependence of the parameters by means of a thermal feedback network. The feedback network is built by exploiting a very effective analytical approach which reduces computational efforts and allows an automated solution. The cell-level discretization allows the description of the temperature distribution over solar cell surfaces in panels subject to mismatch events (e.g., partial shading, localized soiling, etc.), along with its time evolution. Experiments performed on a partially shaded solar string evidence good agreement with the model. In uniform condition the temperature error is less than 3 °C, while, under mismatch, the error on the maximum temperature of a cell subject to hot spot is limited to 5 °C.

1. Introduction

Normally operating Photovoltaic (PV) modules are inherently subject to strong temperature variations; in fact, about 35% of the impinging solar irradiance is directly converted into heat (Green, 1982). The consequence is that, depending on the season, the hour of the day, the presence of clouds, the wind speed and so on, the operating temperature of a solar module can spread (sometimes very suddenly) over a range of tens of Celsius degree. Moreover, since solar modules can be subject to uneven irradiance conditions, non-uniform temperature distributions can be easily found. As it is widely known, the latter occurrence can be strongly amplified when a solar cell of the module gets reverse biased, giving rise to the formation of "hot spots", whose temperature can exceed 100 °C.

The over-temperature in solar panels significantly affects power production, while the occurrence of hot spots can lead to early aging, and even dramatic failures; therefore, reliable modeling of solar systems performance should properly account for thermal effects. The main issue to be faced toward this goal depends on the feedback action that the temperature produces on the electrical power delivered by solar cells which, in turn, affects the temperature. In other terms, the temperature cannot be considered as a fixed external parameter when electrical performance are evaluated. This strict interaction can be accounted for by adopting the electro-thermal approach, which means that the parameters of the electrical network are dynamically changed depending on the temperature, and the temperature is dynamically determined depending on the electrical power dissipated by each element of the electrical network.

Generally speaking, a suitable model accounting for thermal effects should provide the following features: (i) cell level discretization (in order to describe effects related to partial shading of modules, such as hot spot); (ii) inclusion of bypass diodes (in order to correctly describe the behavior of the whole solar panel); (iii) dynamic capability (in order to reproduce thermal transient occurring in the presence of varying boundary conditions).

In the recent literature, many papers dealing with the modeling of thermal effects in solar modules can be found. In (Kim et al., 2011), a temperature dependent solar panel model was presented; however, the solar panel was modeled as a whole, so that localized overheating caused by partial shading cannot be observed (Kim and Krein, 2015).

A single cell electro-thermal model was proposed in (Maffezzoni and D'Amore, 2009) but only the temperature dependence of the inherent solar cell diode was considered.

In (Usama Siddiqui et al., 2012) a FEM numerical simulator was adopted to describe the behavior of a solar panel, also in presence of forced cooling. Although a single cell model was adopted electro-thermal effects were not accounted for, as well as in (Armstrong and Hurley, 2010), (Maràndа and Piotrowicz, 2010), where the authors adopted a panel level discretization. A further drawback of many of the approaches presented so far is the high computational effort, both in terms of computational time and memory requirements.

In the recent literature, thermal maps obtained by IR analysis have

* Corresponding author.
E-mail address: pierluigi.guerriero@unina.it (P. Guerriero).

https://doi.org/10.1016/j.solener.2018.12.067
Received 19 March 2018; Received in revised form 21 September 2018; Accepted 27 December 2018
Available online 06 January 2019
0038-092X/

been exploited to infer information about the operating conditions of solar modules (Hu et al., 2013), thus allowing to implement effective fault detection and classification algorithms (Hu et al., 2014a) and real-time MPPT algorithms (Hu et al., 2014b). The availability of accurate thermal models could favor the improvements in aforementioned applications. In particular, a cell-level approach can correctly take into account the effect of partial shading and hot-spots.

In this paper an electro-thermal model, based on a single cell level granularity, suited to describe the thermal behavior of solar panels under arbitrary uneven (dynamically varying) irradiance conditions, is presented. The model exploits the interaction of an electrical network with a thermal feedback block, whose role is to dynamically adjust the temperature depending parameters of the electrical network. The electrical network is solved by means of a SPICE-like simulator, which is much faster and more accurate than MATLAB/Simulink based approaches. The thermal feedback block contains an equivalent electrical circuit describing the thermal behavior of the solar panel, including the thermal coupling among cells. The parameters of the thermal network are determined in a pre-processing step where the actual 3-D geometries of the solar panel, along with materials properties, are accounted for. More specifically, the commercial software package COMSOL was adopted to build the 3D model of the solar panel, while an in house software (Codecasa et al., 2014) was adopted to extract, from the COMSOL mesh, the corresponding equivalent thermal network.

It is worth noting that, in principle, COMSOL could be exploited to solve the full electro-thermal problem. However, the enormous number of independent power generators (the solar cells) embedded in a solar system would make the computational time absolutely impractical. On the contrary, the adoption of a SPICE like program for solving the electrical networks, once reliable parameters have been provided, makes the simulation very fast and accurate.

In the proposed model each solar cell is described by means of an equivalent subcircuit (based on the single diode solar cell model) accounting for the temperature dependence of all relevant parameters. A proper number of subcircuits are series connected to describe actual solar panels. Thermal gradients over the solar panel are evaluated by taking into account the power generated by each solar cell. Bypass diodes are also included in the circuit, so that critical phenomena, such as the formation of hot spots, can be effectively described.

The paper is organized as follows: in Section 2 the electrical macrocircuit for the solar cell is presented, along with analytical models describing temperature dependencies of solar cell parameters. Section 3 describes the thermal feedback block. Numerical results are reported in Section 4, while in Section 5 some experiments are commented. Conclusions are drawn in Section 6.

2. The electro-thermal macrocircuit

As outlined above, the electrio-thermal model (*macrocircuit*) of a photovoltaic system can be built by interconnecting a proper number of *subcircuits* representing the elemental solar cells and by integrating a thermal feedback block. The model adopted in this paper is show in Fig. 1, where the electrical subcircuit and the associated thermal feedback block are reported.

The basic structure of the *subcircuit* is the same of the widely known single diode equivalent circuit; in addition, nonlinear sources are exploited to take into account the dependencies of the parameters upon temperature, irradiance and reverse voltage.

In this regard, it should be pointed out that SPICE like programs do not allow changing the temperature during a simulation run (the electrical network is always solved at a fixed reference temperature T_0), while time varying current and voltage sources are allowed. In the proposed approach, the actual temperature of the circuit is associated to the instant value of the nonlinear sources embedded in the *subcircuit*.

In other terms, the thermal equivalent of the Ohm's law (by which temperatures and powers are represented with voltages and currents, respectively) is adopted to associate a different temperature to each cell while simulations are always performed at the reference temperature.

More specifically, as can be seen from Fig. 1, one of the output of the *subcircuit* is the power P_{cell} generated by the solar cell at a given temperature; this power is supplied as input to the thermal feedback block, that evaluates the temperature increment (or decrement) ΔT corresponding to that power. ΔT is, in turn, supplied to the subcircuit (in the form of a voltage that drives the controlled sources) which evaluates the new value of the output power. Iterations continue until convergence is reached.

It is important to notice that, as will be clarified in the next section, the thermal feedback block contains the equivalent thermal circuit of the whole solar panel; thus, the new temperature of one cell is evaluate by accounting for both the self-heating and the mutual thermal interaction among all solar cells and taking into account proper boundary conditions (wind speed and so on). The latter point is very important because, differently from electro-thermal modeling of standard electronic devices, solar panels are subject to nonlinear boundary conditions (more details on this point in Section 3.1).

As can be seen from Fig. 1 the *subcircuit* contains five controlled sources (indicated as A, B, C, D, E in the figure) accounting for temperature dependent parameters. The models implemented for each of them are described below.

2.1. The photogenerated current source A

The formulation adopted for the photogenerated current I_{ph}, as a function of the irradiance G and the temperature T, is

$$I_{ph} = I_{sc_{nom}} \cdot \frac{G}{G_{nom}} + I_{sc_{nom}} \cdot \alpha \cdot \Delta T \tag{1}$$

where $I_{sc_{nom}}$ is the short circuit current under standard test conditions (STC, i.e. $G_{nom} = 1000\ \mathrm{W/m^2}$ and $T = 25\ ^\circ\mathrm{C}$), and α is the normalized temperature coefficient of the photocurrent (both $I_{sc_{nom}}$ and α can be read on the panel datasheets).

The procedure to evaluate I_{ph} for each solar cell can be explained as follows. The distribution of the irradiance over the solar panel is determined by invoking specific routines accounting for day of the year, true local time, relative position of the panel with respect to Sun, and shadow patterns (in this work an *in house* program (d'Alessandro et al., 2015) accounting for small shadows was exploited); I_{ph} (G, 25 °C) is consequently evaluated for each cell and provided to the corresponding *subcircuit*; then, the actual photocurrent is calculated within the *subcircuit* by the nonlinear source I_{ph} (G,T) (see A in Fig. 1) which adds $I_{sc_{nom}} \cdot \alpha \cdot \Delta T$ to I_{ph} (G, 25 °C), with ΔT provided by the thermal feedback block.

2.2. The intrinsic diode current source B

The description of the temperature dependence of the diode current (I_D(T) in Fig. 1) is one of the key points for achieving a reliable electro-thermal simulation of the solar cell. For this reason, the model proposed in this paper is described in detail. It is based on the well-known Shockley equation of the diode current I_D

$$I_D = I_0 \cdot \left[\exp\left(\frac{V_D}{n V_T} \right) - 1 \right] \tag{2}$$

where I_0 is the reverse saturation current, n is the ideality factor and $V_T = kT/q$ is the thermal voltage, T being the junction temperature and $k = 8.62 \times 10^5$ eV/K the Boltzmann's constant. The current I_D increases with temperature due to the prevailing positive temperature coefficient of I_0. The current I_0 can indeed be expressed as

$$I_0(T) \approx qA \cdot \frac{V_T \mu_n(T)}{L_n N_A} \cdot n_i^2(T) \tag{3}$$

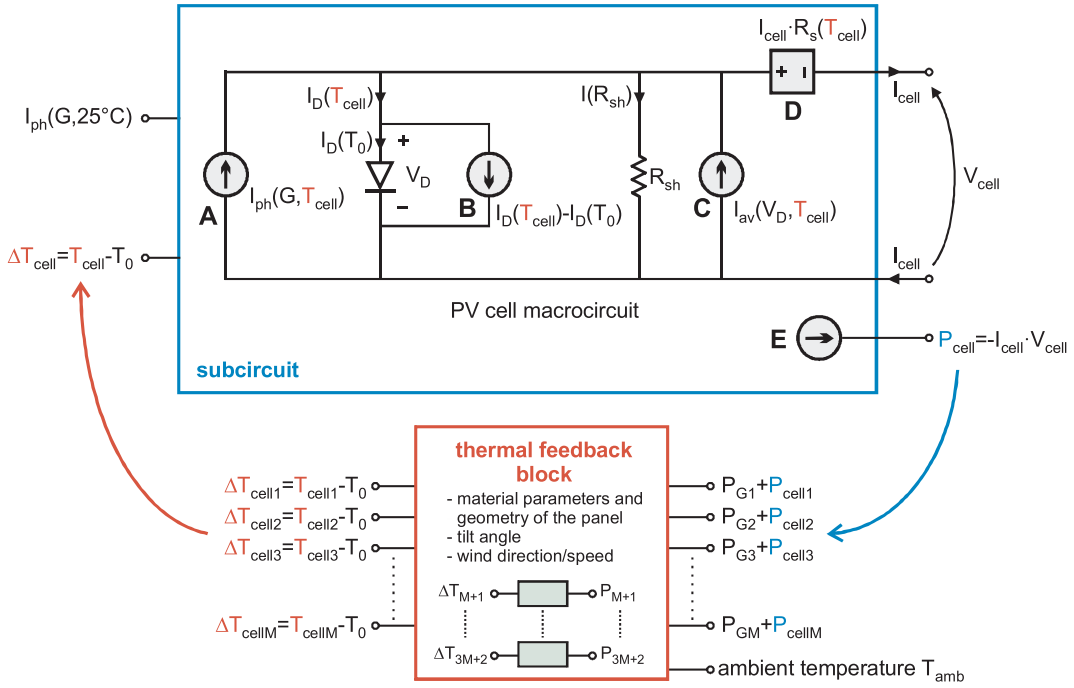

Fig. 1. Schematic macromodel for a PV cells evidencing the controlled sources and the Thermal Feedback Block.

where A is the diode area, N_A is the acceptor doping, L_n is the electron diffusion length (which can be reasonably assumed to be temperature-insensitive), μ_n is the electron mobility, and n_i is the intrinsic carrier concentration. The electron mobility depends upon temperature according to (Sze and Kwok, 2007)

$$\mu_n(T) = \mu_n(T_0)\left(\frac{T}{T_0}\right)^{-\frac{3}{2}} \tag{4}$$

where $T_0 = 300\,\mathrm{K}$. Furthermore, it can be demonstrated that

$$n_i^2(T) = BT^3 \cdot \exp\left(-\frac{V_{g0}}{V_T}\right) \tag{5}$$

where B is a parameter independent of the temperature, and V_{g0} is the voltage-equivalent silicon bandgap extrapolated at $T = 0\,\mathrm{K}$ ($\approx 1.21\,\mathrm{V}$). By substituting (4) and (5) into (3), it is found that

$$I_0(T) = CT^{2.5} \cdot \exp\left(-\frac{V_{g0}}{nV_T}\right) \tag{6}$$

where C collects all the temperature-insensitive terms. Subsequently, by replacing (6) into (2) and neglecting unity compared to the exponential, the following relation, illustrating the temperature dependence of I_D is achieved:

$$I_D(T) = CT^{2.5} \cdot \exp\left(\frac{V_D - V_{g0}}{nV_T}\right) \tag{7}$$

It follows that V_D can be expressed as

$$V_D = V_{g0} - nV_T \ln\left(\frac{CT^{2.5}}{I_D}\right) \tag{8}$$

Let us denote as ϕ (> 0) the absolute value of the temperature coefficient of the voltage V_D for an assigned current I_D, that is,

$$\phi = -\left.\frac{\partial V_D}{\partial T}\right|_{I_D} \tag{9}$$

By making use of (8), it is obtained that

$$\phi = n\frac{k}{q} \cdot \left[2.5 + \ln\left(\frac{CT^{2.5}}{I_D}\right)\right] \approx n\frac{k}{q} \cdot \left[2.5 + \ln\left(\frac{CT_0^{2.5}}{I_D}\right)\right] \tag{10}$$

the approximation $T \approx T_0$ being reasonable in a wide range of temperatures (Sze and Kwok, 2007). After some algebra (10), can be written as

$$\phi(I_D) = \phi_0 - n\frac{k}{q} \cdot \ln\left[\frac{I_D}{I_0(T_0)}\right] \tag{11}$$

where ϕ_0 is a constant given by

$$\phi_0 = n\frac{k}{q} \cdot \left\{2.5 + \ln\left[\frac{CT_0^{2.5}}{I_0(T_0)}\right]\right\} \tag{12}$$

From this analysis, it can be concluded that V_D, for a given current I_D, can be expressed as

$$V_D(T)|_{I_D} = V_D(T_0)|_{I_D} - \phi(I_D) \cdot \Delta T \tag{13}$$

ϕ being a function of I_D according to (11). Relation (13) allows obtaining, by exploiting (2), the following implicit function:

$$I_D = I_0(T_0) \cdot \exp\left[\frac{V_D(T) + \phi(I_D) \cdot \Delta T}{nV_{T0}}\right] \tag{14}$$

with $V_{T0} = kT_0/q$. By substituting (11) into (14), the dependence of the right side on the diode current I_D is eliminated

$$I_D = I_0(T_0) \exp\left(\frac{V_D + \phi_0 \cdot \Delta T}{nV_{T0} + n\frac{k}{q} \cdot \Delta T}\right) \tag{15}$$

thus providing an expression of the diode I-V curve with the dependence on the temperature increment ΔT explicitly visible.

Formulation (15) was implemented in the subcircuit by dividing the contribution given by the standard SPICE diode, which conducts the current $I_D(T_0)$ (since the whole circuit is kept at T_0) and a parallel nonlinear current source that forces $I_D(T)$-$I_D(T_0)$ (see B in Fig. 1), where $I_D(T)$ is given by (15); consequently the total current in the diode branch is equal to $I_D(T)$ (see Fig. 1).

2.3. Impact ionization current source C

Solar panels subject to partial shading are prone to reverse biasing of the P-N junctions. Therefore, impact ionization mechanics must be taken into account. In this paper, an extension of the Bishop model (Bishop, 1988) is adopted. The total cell current I_{cell} is considered as given by the sum of the current that would flow in the absence of impact ionization and an avalanche current I_{av} given by

$$I_{av} = -\frac{V_D}{R_{sh}} a \left[1 - \frac{V_D}{BV(T_{ell})}\right]^{-m} \tag{16}$$

where R_{sh} is the shunt resistance of the cell (R_{sh} is considered temperature insensitive; specific models, such as (Banerjee and Anderson, 1986), could be implemented) coefficients a and m are dimensionless fitting parameters, and BV (< 0 V) is the breakdown voltage of the P-N junction, whose dependence on temperature can be written as

$$BV(T) = BV(T_0) \cdot \exp(b \cdot \Delta T) \tag{17}$$

where b is a fitting parameter as well.

2.4. The series resistance voltage drop source D

In the subcircuit depicted in Fig. 1, the series resistance R_s accounts for the contribution of both the semiconductor (bulk and emitter regions) and metallic lines (fingers and bus bars). In the proposed approach, the effect of metallic lines on series resistance is assumed to be negligible, and R_s is assumed to have a power law dependence on temperature,

$$R_s(T) = R_s(T_0) \cdot \left(\frac{T_0 + \Delta T}{T_0}\right)^{m_R} \tag{18}$$

where T_0 is expressed in Kelvin degrees, and $m_R > 0$.

The voltage drop $I_{cell}R_s(T)$ caused by R_s is computed by a voltage controlled source which accepts the temperature rise ΔT and the current I_{cell} as inputs, and imposes the drop.

More accurate results can be obtained by adding in the circuit a second lumped series resistor accounting for the contribution of the metallic lines, thus being subject to a linear dependence on temperature.

2.5. The output power controlled source E

The output power produced by the cell is simply calculated by multiplying I_{cell} by V_{cell}. According to the thermal equivalent of the Ohm's law, the numerical value thus obtained is supplied to the thermal feedback block in the form of a current.

3. Thermal feedback block

The dynamic power-temperature feedback is modeled, for each solar panel, by means of an equivalent compact electrical network, denoted as Thermal Feedback Block (TFB). The TFB is built in a pre-processing, merely-thermal analysis, through the following procedure.

3.1. COMSOL structure

The commercial software package COMSOL ("Comsol 3.5a, User's Manual," 2008) was exploited for representing the 3-D structure of the solar panel on the basis of information about both geometries and material parameters (mainly taken from the datasheet).

The solar panel ET-M54050A ("ET-M54050, datasheet,") was taken as case study; its geometry and the corresponding values are reported in Fig. 2 and Table 1, respectively. Thermal parameters (mass density ρ, specific heat c, thermal conductivity k) describing the thermal behavior of the solar panel are reported in Table 2, while electrical parameters characterizing the models described in Section 2 can be found in Table 3.

The commercial module shown in Fig. 2 was drawn in the COMSOL environment; a detail of the corresponding mesh is shown in Fig. 3.

As mentioned above, COMSOL was exploited to solve the thermal problem, whose formulation is discussed in the following. The solar panel was assumed to be mounted with a tilt angle β with respect to the horizontal plane, subject to wind and sunlight. Both free and forced convective mechanisms of energy exchange, along with the radiative mechanism, were taken into account.

Forced convection (depending on wind speed) was modeled by means of the heat transfer coefficient h_{forced}, while h_{free} is the free heat transfer coefficient.

Since the top surface of the panel was assumed to be subject to the incident wind, the total heat transfer coefficient h_{front} accounting for both free and forced convection on the front was determined as (Armstrong and Hurley, 2010)

$$h_{front} = \sqrt[3]{h_{free}^3 + h_{forced}^3} \tag{19}$$

Conversely, the rear surface was assumed to be shielded from the wind, i.e., only free convection was considered, resulting in the following expression of total heat transfer coefficient h_{rear}

$$h_{rear} = h_{free} \tag{20}$$

Radiative thermal exchange was considered from both front and rear surfaces. The power densities q_{rad} [W/m^2] exchanged between the front surface and the ambient, and the rear side and the ambient, were evaluated as (Armstrong and Hurley, 2010)

$$q_{rad,front} = F_{front}\varepsilon_{front}\sigma(T_{front}^4 - T_{ambient}^4) \tag{21}$$

$$q_{rad,back} = F_{back}\varepsilon_{back}\sigma(T_{back}^4 - T_{ambient}^4) \tag{22}$$

where ε is the emissivity, and σ [W/m^{2}K^4] is the Stephan-Boltzmann constant. The terms F_{front} and F_{back} are the *front to sky* and *back to ground* view factors, respectively expressed as

$$F_{front} = \frac{1 + \cos\beta}{2} \tag{23}$$

$$F_{back} = \frac{1 - \cos(180 - \beta)}{2} \tag{24}$$

Side surfaces were assumed adiabatic, i.e. the thermal exchange through them was assumed negligible due to their small dimensions with respect to the top and bottom surfaces.

3.2. Equivalent thermal network

The COMSOL environment allowed the extraction of the equivalent thermal feedback network, where each one of the N solar cells acts as a thermal source providing a power corresponding to the part of the incident radiation not converted into electrical power. The cell temperature depends on both self and mutual heating.

In principle, two approaches could have been exploited.

The first one, more intuitive, is based on the Foster RC network (Merrikh and McNamara, 2014). In such an approach, the heat conduction in the solar panel is modeled as a linear problem and solved by means of N electrical networks, shown in Fig. 4, where the resistances R_{ij} represent the conductive thermal exchanges among solar cells, while the capacitances C_{ij} account for dynamic effects. In particular, the index "i" refers to the solar cell whose temperature increment is to be evaluated, while the index "j" refers to the thermal sources (i.e., solar cells) generating the thermal power P_j.

As an example, by referring to the circuit at the very left in Fig. 4, the current P_1 is the thermal power generated inside cell #1; the RC pair with subscript "11″ models the self-heating occurring in cell #1 (the effect of cell #1 on cell #1); the pairs with subscript "i1″ account

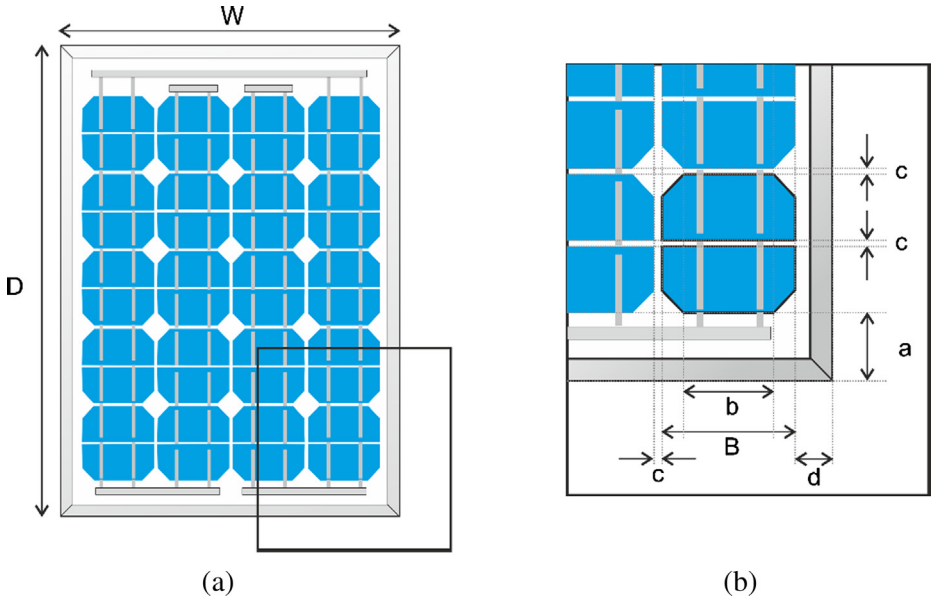

Fig. 2. Technical drawing of the solar panel ET-M54050A: (a) panel external dimensions, (b) details of cells placement.

Table 1
Geometric parameters of the PV panel depicted in Fig. 1.

Thickness	[mm]
Glass	3
EVA	0.95
Si cell	0.15
Back	1
Module	
D	719
W	555
Cell	
B	127.25
b	82
Spacing	
a	32
d	20
c	2

Table 2
Physical parameters of materials.

	ρ [kg/m^3]	*c* [J/kg K]	*k* [W/mK]
Glass	3000	500	1.8
EVA	960	2090	0.35
Si cell	2330	677	148
Back	1200	1250	0.15

Values of the material parameters (mass density ρ, specific heat *c*, thermal conductivity *k*).

Table 3
Model parameters of solar cells.

Parameter	Value
I_{scnom}	2.8 A
α	0.06%/K
$I_0(T_0)$	8 nA
n	1.2
ϕ_0	4.4 mV/K
$BV(T_0)$	−10 V
a	0.1
m	1.1
R_{sh}	100 Ω
$R_s(T_0)$	12 mΩ
m_R	1.5

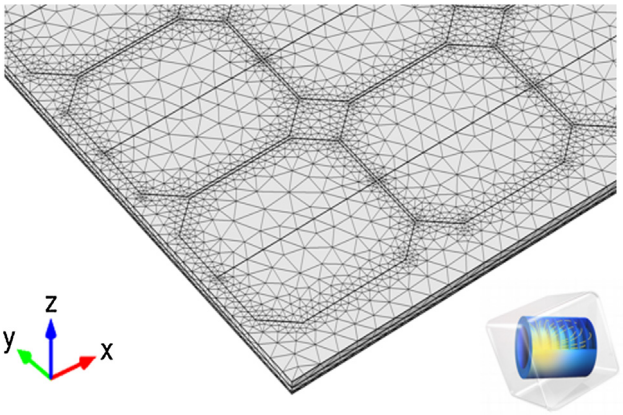

Fig. 3. Detail of the COMSOL mesh.

for the heating of cell #i due to the power generated in cell #1. Other terms can be straightforwardly interpreted.

By applying the superposition effects, the total increment of temperature in cell #1 is given by the following expression:

$$\Delta T_1 = \sum_{j=1}^{N} v_{1j} \tag{25}$$

where v_{1j} is the voltage across the RC pair "1*j*", representing the temperature increment in cell #1 due to the *j*-th thermal source.

The implementation of the Foster's network encounters two main issues. First, a single RC pair is usually not sufficient, because thermal phenomena occurring in solar panels cannot be described by means of a single time constant (this is particularly true for self-heating which is the dominant term), moreover the number of pairs needed for a reliable description cannot be defined a priori. Second, the procedure for determining the parameters of the thermal network is very time consuming. In fact, each term should be singularly determined by performing simulated experiments consisting in "turning on" one cell at time and evaluating the time dependent mutual thermal impedances of all other cells; after that, the coefficients of the Foster's network can be

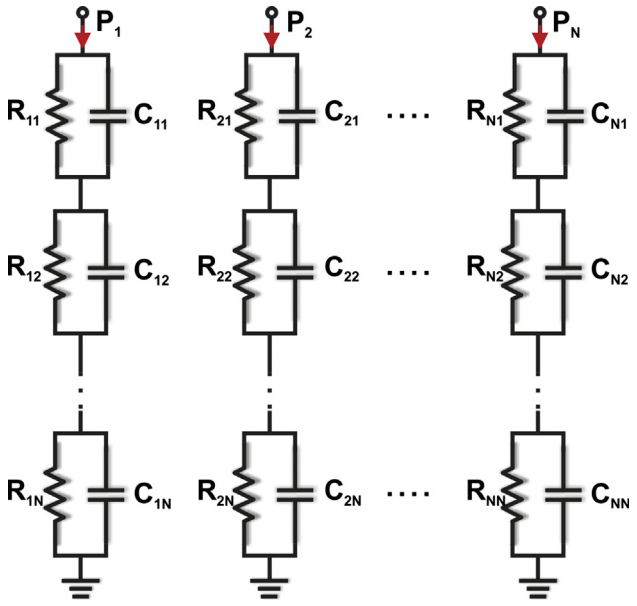

Fig. 4. Foster RC thermal network.

determined by means of the Jakopovic procedure (Jakopović et al., 1990).

In this paper the Multi-Point Moment Matching Algorithm (MPMMA) proposed in (Codecasa et al., 2005), and already exploited in (Codecasa et al., 2014) for the thermal modeling of microelectronic devices, has been extended to solar panels. The MPMMA strongly reduces the order of the mathematical problem; moreover, it allows an equivalent of the Foster network (generalized Foster network) whose parameters can be rigorously evaluated by direct analysis of the COMSOL mesh, without performing simulated experiments. Details of the MPMMA formulation are given in (Codecasa et al., 2005) and, for the sake of brevity, are not repeated here. The form (referring to only one solar cell) of the generalized Foster network achieved for the structure of Fig. 3 is shown in Fig. 5.

As can be seen there are N-1 voltage-controlled current sources that account for temperature increment of cell #1 due to the power generated into cells #2 … #N (in place of N-1 RC pairs).

It is worth noting that the adopted approach identifies a linear transformation determining the temperature of each node of the mesh. In other words, the same transformation allowing to identify the equivalent Foster network, starting from the mesh points, can be exploited to determine the temperature of the mesh points starting from the solutions of the thermal network (Codecasa et al., 2005). Therefore, the final outputs of the model are the detailed temperature maps shown in the next section (see Fig. 12).

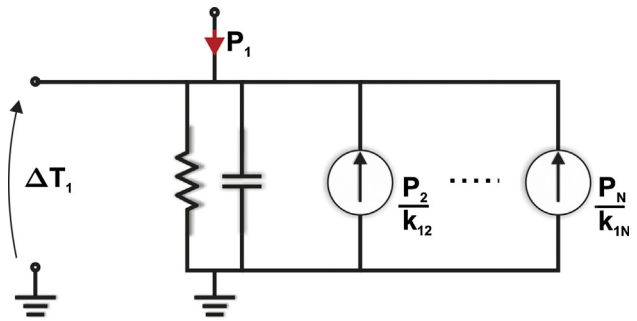

Fig. 5. Simplified form (referring to only one cell, modeled with a single RC pair) of the generalized Foster network.

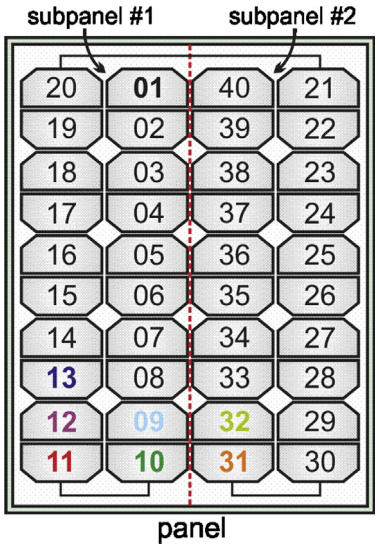

Fig. 6. Cell numbering of the solar panel.

4. Dynamic simulations

The above model was exploited to determine the dynamic behavior, both electrical and thermal, of a solar panel embedded in a string subject to a moving shadow.

A PV string made by 10 solar panels was considered. The electrical circuit and the thermal feedback network describing the behavior of individual panels were calibrated on the commercial panel ET-M54050A, whose technical specifications are reported in Section 3. Parameters and boundary conditions were properly adjusted to emulate the operating conditions of the 10-panel (ET-M54050A) string used in the experimental tests discussed in the next section, thus ensuring a fair comparison between numerical and experimental results.

The ET-M54050A solar panel is made by two subpanels, each composed by 20 monoSi cells “protected” by a bypass diode. For illustrative purpose, the adopted numbering of the cells is reported in Fig. 6 (note that each solar cell is made by half silicon wafer).

For the case study, 9 solar panels in the string were kept unshaded, while a single panel was subject to a dynamic shadowing in the interval of time 0–3600 s. The pattern of the shadow emulated the one actually implemented for the experiments; in Fig. 7 such patterns (real photos), at three key time instants, are shown. It must be remarked that the shadow only prevented direct radiation from reaching solar cells, while the diffused component of the light contributed to the photogenerated current; in other terms, the current provided by a completely shaded solar cell was not neglected.

As it is widely known, uneven irradiation patterns, like those shown in Fig. 7, lead to the activation of bypass diodes (Daliento et al., 2016) and, as a consequence, to a strong distortion of the power-voltage curve, with the appearance of multiple maximum power points (Guerriero et al., 2015). The I-V curves evaluated by the model at t = 0 s (no shadow), t = 450 s (cell #11 slightly shaded), t = 900 s (a fourth of cell #11 shaded), t = 1800 s (cell#11 fully shaded), and t = 2700 s (cells #10 and #11 fully shaded) are shown in Fig. 8. It is worth noting that (as in the experiments) simulations accounted for the operation of a Perturb&Observe (P&O) Maximum Power Point Tracking (MPPT) algorithm, forcing the operating point of the string to dynamically follow the maximum power point. As can be argued from Fig. 8, in the first interval of time, the bypass diode of subpanel #1 was not yet conducting; while, after t = 900 s, the MPPT algorithm bypassed the subpanel.

The evolution of the key currents of the subpanel #1, reported in Fig. 9, and the voltages across the shaded cells, reported in Fig. 10, offer

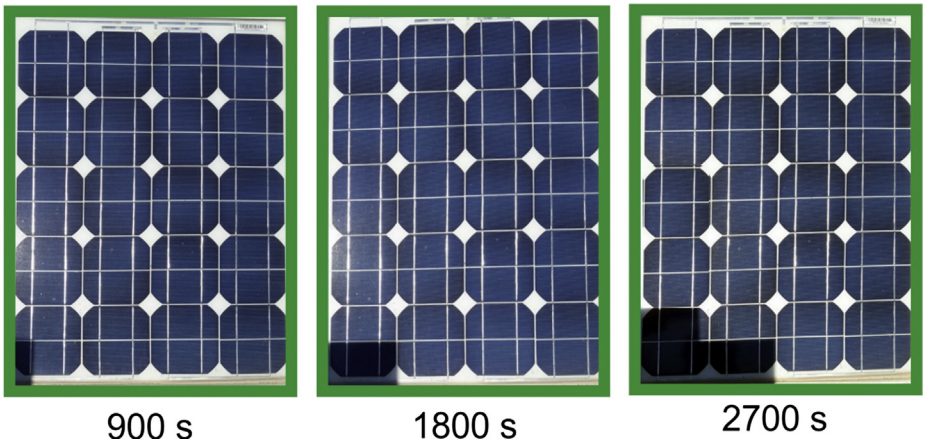

Fig. 7. Photograph of shadow pattern at three key instants.

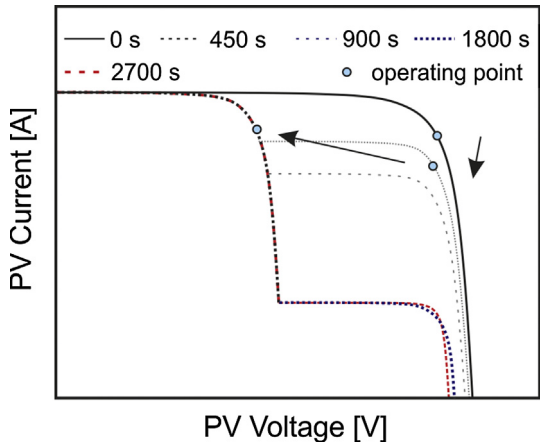

Fig. 8. Simulated I-V curves at various instants. The route of the operating points, as determined by the MPPT algorithm, is shown.

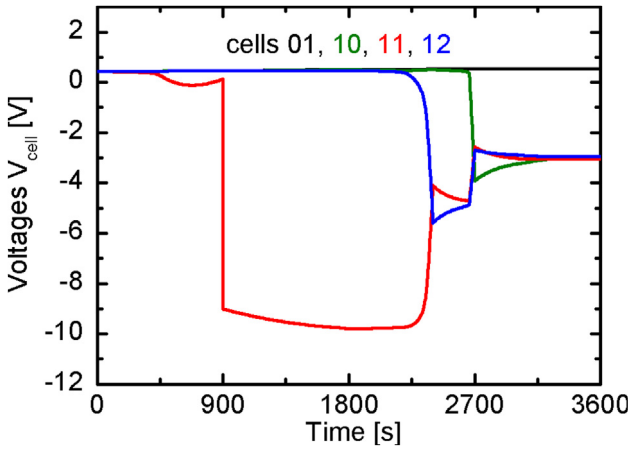

Fig. 10. Simulated evolution of voltage across solar cells subject to partial shading.

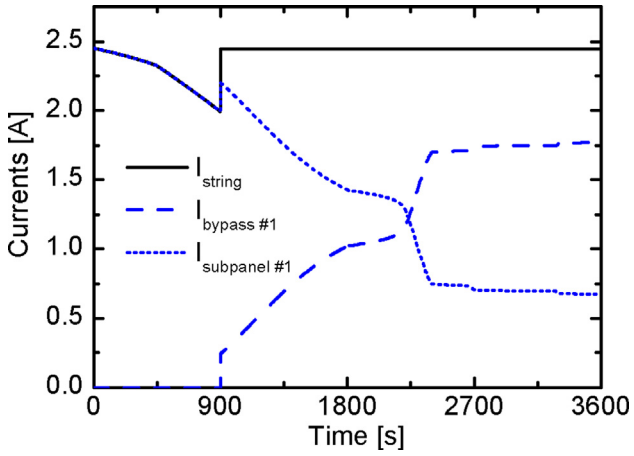

Fig. 9. Simulated evolution of the currents in the partially shaded submodule.

an easy diagnosis of the shadow impact. Between 0 s and 900 s, the corner cell #11 is progressively obscured, thus reducing the string current I_{string} (see the operating points in Fig. 8). At t = 900 s, due to the further decrease of the current provided by subpanel #1, the MPPT algorithm identifies a new global maximum, thus reducing the operating voltage of the string and causing the turning on of the bypass diode of subpanel #1. At the same time cell #11 gets reverse biased (see Fig. 10). As the shadow over cell #11 enlarges, $I_{subpanel\#1}$ reduces, while the current $I_{bypass\#1}$, flowing through the bypass diode, grows (the sum being equal to I_{string}).

At t = 2350 s, cell #12 was also reversed, thus sharing part of the reverse voltage which was previously sustained only by the cell #11 (about 10 V).

Since the product between currents and voltages is the power delivered or absorbed (depending on the sign of the voltage) by the solar cells, the power plots shown in Fig. 11a have the thermal counterpart shown in Fig. 11b, where the average temperature evaluated over the cells during the shading events are shown.

Since the temperatures are available for each point of the COMSOL mesh, the detailed temperature maps corresponding to selected instants of time can be plotted as well, as shown in Fig. 12.

The above figures can be interpreted as follows. The reverse biasing of cell #11 occurring at t = 900 s implies that cell #11 starts *dissipating* power, thus heating up under weak avalanche conditions. Consequently, its temperature suddenly increases. The subsequent enlarging of the shadow causes the reduction of $I_{subpanel}$ (see Fig. 9) so that the power dissipated by the cell decreases, and the temperature, after reaching the maximum of about 90 °C at 1400 s, starts reducing. It should be remarked that the model correctly predicts that the temperature of cell #12 – which is still *generating* power – increases due to its close proximity to cell #11. With the enlarging of the shadow more solar cells get reverse biased, thus sharing the voltage provided by the sunny cells. As a consequence, the electrical dissipated power decreases and the shaded solar cells cool down, by reaching a temperature lower than that found on the unshaded cells.

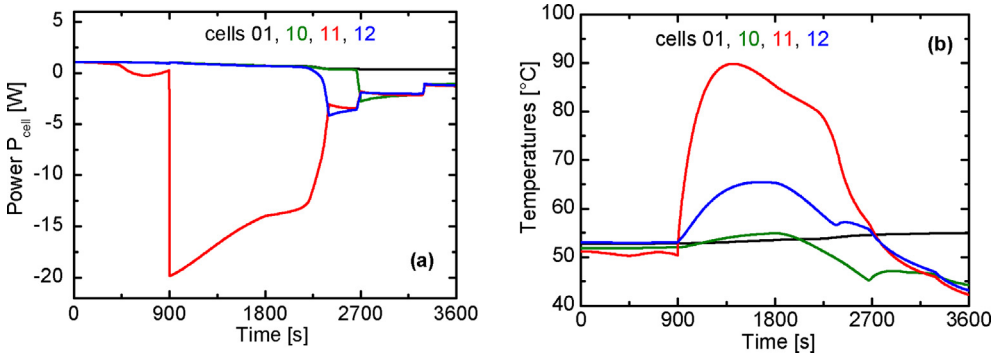

Fig. 11. Simulated evolution of (a) power and (b) average temperature corresponding to solar cells subject to partial shading.

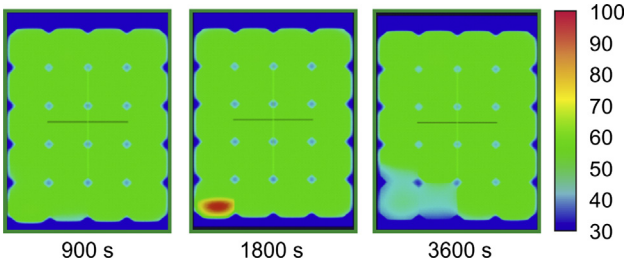

Fig. 12. Temperature maps at three key instants.

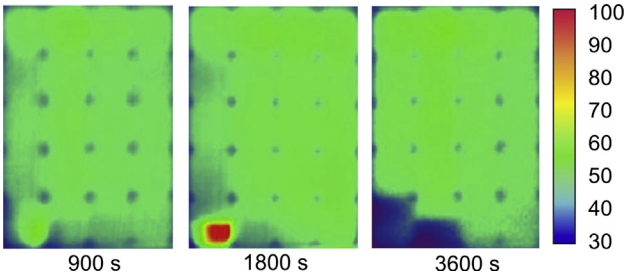

Fig. 13. Experimental thermal maps corresponding to the same shading conditions analyzed in Fig. 12.

5. Experiments

The behavior described in the previous section was experimentally verified. The first solar panel of a PV string made by 10 series connected solar panels (ET-M54050A) was intentionally shaded by a moving shield producing the shadow patterns already shown in Fig. 7.

A thermo-camera HT THT70 (384 × 288 pixels) was exploited to obtain the temperature maps of the shaded panel. The camera was installed 3 m far from the shaded panel and a thermocouple was used to perform a preliminary calibration. To avoid undesired shadow of the PV modules and the reflection of the sunlight, the camera direction was not normal to the surface of the module. In a post processing step, a Gaussian filter was applied to the thermal images to reduce the quantization effect, while the perspective error was corrected by means of a homemade procedure in order to obtain experimental thermal maps easily comparable with the numerical results.

Thermographic images, corresponding to the same key instants of Fig. 12, are reported in Fig. 13. As can be seen a remarkable agreement with simulations can be observed, thus proving the reliability of the proposed model.

The model effectively describes the considered shading event in terms of temperature behavior.

Under uniform irradiance conditions, the discrepancy between numerical and experimental results in terms of mean temperature over individual cells is within 3 °C.

As the shadow moves to partially impacting the cell #11, the model correctly predicts the occurrence of a hot spot, estimating a maximum temperature of about 90 °C with an error of about 5 °C with respect to experimental results. Nevertheless, the shape of the temperature distribution over the cell slightly differs from experiments. Indeed, experimental results show, in cell #11, an increase in temperature limited to the unshaded portion of the cell. On the contrary, the model, based on one-cell level macrocircuit, hence considering uniform distribution of the dissipated power over the cell, shows an increase in temperature spreading over the whole cell.

Finally, as the shadow impacts on a significant number of cells, thus making them share the power dissipation, the model well predicts that these cells cool down with respect to the others. A slightly mismatch concerning the temperature distribution over cell 11# between numerical and experimental results is mainly due to the inherent limit of the cell-level electrical model, only allowing uniform power distribution on the cell. This effect is more visible during the cooling of shaded cells, when the predominant contribution of the sunlight is absent.

6. Conclusions

This paper describes an effective electro-thermal model able to foresee the time dependent temperature distribution over solar panel subject to varying, uneven, irradiance conditions. The approach relies on a very efficient mathematical procedure that receives as input the numerical representation of the actual structure of the solar panel and automatically generates an electrical equivalent *macrocircuit*, which can be solved by circuit simulators. The high level of discretization allows identifying the conditions leading to the appearance of the hot spot and to estimate the temperature reached by the hot cells. The reliability of the model has been evidenced by comparing numerical results with experiments. Under uniform irradiation conditions, simulated results meet experiments with an error on the mean temperature of the individual cell within 3 °C, and correctly predicts the occurrence of hot spots in a partially shaded cell (5 °C error on the maximum temperature).

References

Armstrong, S., Hurley, W.G., 2010. A thermal model for photovoltaic panels under varying atmospheric conditions. Appl. Therm. Eng. 30, 1488–1495. https://doi.org/10.1016/j.applthermaleng.2010.03.012.

Banerjee, S., Anderson, Weston A., 1986. Temperature dependence of shunt resistance in photovoltaic devices. Appl. Phys. Lett. 49, 38. https://doi.org/10.1063/1.97076.

Bishop, J.W., 1988. Computer simulation of the effects of electrical mismatches in photovoltaic cell interconnection circuits. Sol. Cells 25, 73–89.

Codecasa, L., D'Alessandro, V., Magnani, A., Rinaldi, N., Zampardi, P.J., 2014. FAst Novel Thermal Analysis Simulation Tool for Integrated Circuits (FANTASTIC). In: 20th INTERNATIONAL WORKSHOP on Thermal Investigations of ICs and Systems. Greenwich, London, UK.

Codecasa, L., D'Amore, D., Maffezzoni, P., 2005. Multipoint moment matching reduction from port responses of dynamic thermal networks. IEEE Trans. Components Packag. Technol. 28, 605–614. https://doi.org/10.1109/TCAPT.2005.859741.

Comsol 3.5a, User's Manual, 2008.

d'Alessandro, V., Di Napoli, F., Guerriero, P., Daliento, S., 2015. An automated high-granularity tool for a fast evaluation of the yield of PV plants accounting for shading effects. Renew. Energy 83, 294–304.

Daliento, S., Di Napoli, F., Guerriero, P., d'Alessandro, V., 2016. A modified bypass circuit for improved hot spot reliability of solar panels subject to partial shading. Sol. Energy 134. https://doi.org/10.1016/j.solener.2016.05.001.

ET-M54050, datasheet [WWW Document], n.d. ET-Solar. URL https://www.etsolar.com.ar/folletos/ET-M54050(50w).pdf.

Green, M.A., 1982. Solar cells: operating principles, technology, and system applications. Prentice-Hall Inc, Englewood Cliffs, NJ.

Guerriero, P., Di Napoli, F., D'Alessandro, V., Daliento, S., 2015. Accurate maximum power tracking in photovoltaic systems affected by partial shading. Int. J. Photoenergy.

Hu, Y., Cao, W., Ma, J., Finney, S.J., Li, D., 2014a. Identifying PV module mismatch faults by a thermography-based temperature distribution analysis. IEEE Trans. DEVICE Mater. Reliab. 14, 951–960.

Hu, Y., Cao, W., Wu, J., Ji, B., Holliday, D., 2014b. Thermography-based virtual MPPT scheme for improving PV energy efficiency under partial shading conditions. IEEE Trans. Power Electron. 29, 5667–5672. https://doi.org/10.1109/TPEL.2014.2325062.

Hu, Y., Gao, B., Song, X., Tian, G.Y., Li, K., He, X., 2013. Photovoltaic fault detection using a parameter based model. Sol. Energy 96, 96–102. https://doi.org/10.1016/j.solener.2013.07.004.

Jakopović, Z., Benčić, Z., Končar, R., 1990. Identification of thermal equivalent-circuit parameters for semiconductors. In: Proc. IEEE Computers in Power Electronics, pp. 251–260. https://doi.org/10.1109/CIPE.1990.657945.

Kim, K.A., Krein, P.T., 2015. Reexamination of Photovoltaic Hot Spotting to Show Inadequacy of the Bypass Diode. IEEE J. Photovoltaics 5, 1435–1441. https://doi.org/10.1109/JPHOTOV.2015.2444091.

Kim, J.P., Lim, H., Song, J.H., Chang, Y.J., Jeon, C.H., 2011. Numerical analysis on the thermal characteristics of photovoltaic module with ambient temperature variation. Sol. Energy Mater. Sol. Cells 95, 404–407. https://doi.org/10.1016/j.solmat.2010.05.016.

Maffezzoni, P., D'Amore, D., 2009. Compact electrothermal macromodeling of photovoltaic modules. IEEE Trans. Circuits Syst. II Express Briefs 56, 162–166. https://doi.org/10.1109/TCSII.2008.2011612.

Maràndа, W., Piotrowicz, M., 2010. Extraction of thermal model parameters for field-installed photovoltaic module. 2010 27th Int. Conf. Microelectron. MIEL 2010 - Proc. 153–156. https://doi.org/10.1109/MIEL.2010.5490512.

Merrikh, A.A., McNamara, A.J., 2014. Parametric evaluation of foster RC-network for predicting transient evolution of natural convection and radiation around a flat plate. Thermomech. Phenom. Electron. Syst. -Proceedings Intersoc. Conf. 1011–1018. https://doi.org/10.1109/ITHERM.2014.6892392.

Sze, S.M., Kwok, K.N., 2007. Physics of Semiconductor Devices, third ed. https://doi.org/10.1002/0470068329.

Usama Siddiqui, M., Arif, A.F.M., Kelley, L., Dubowsky, S., 2012. Three-dimensional thermal modeling of a photovoltaic module under varying conditions. Sol. Energy 86, 2620–2631. https://doi.org/10.1016/j.solener.2012.05.034.